Datashare 52:

The petrophysical and petrographical properties of hyaloclastite deposits: Implications for petroleum exploration

Tim J. Watton, Kirstie A. Wright, Dougal A. Jerram, and Richard J. Brown

AAPG Bulletin, v. 98, no. 3 (March 2014), pp. 449–463

APPENDIX 1: WIRELINE LOGS AND DOMINANT MINERALOGY FOR LOG SECTION B

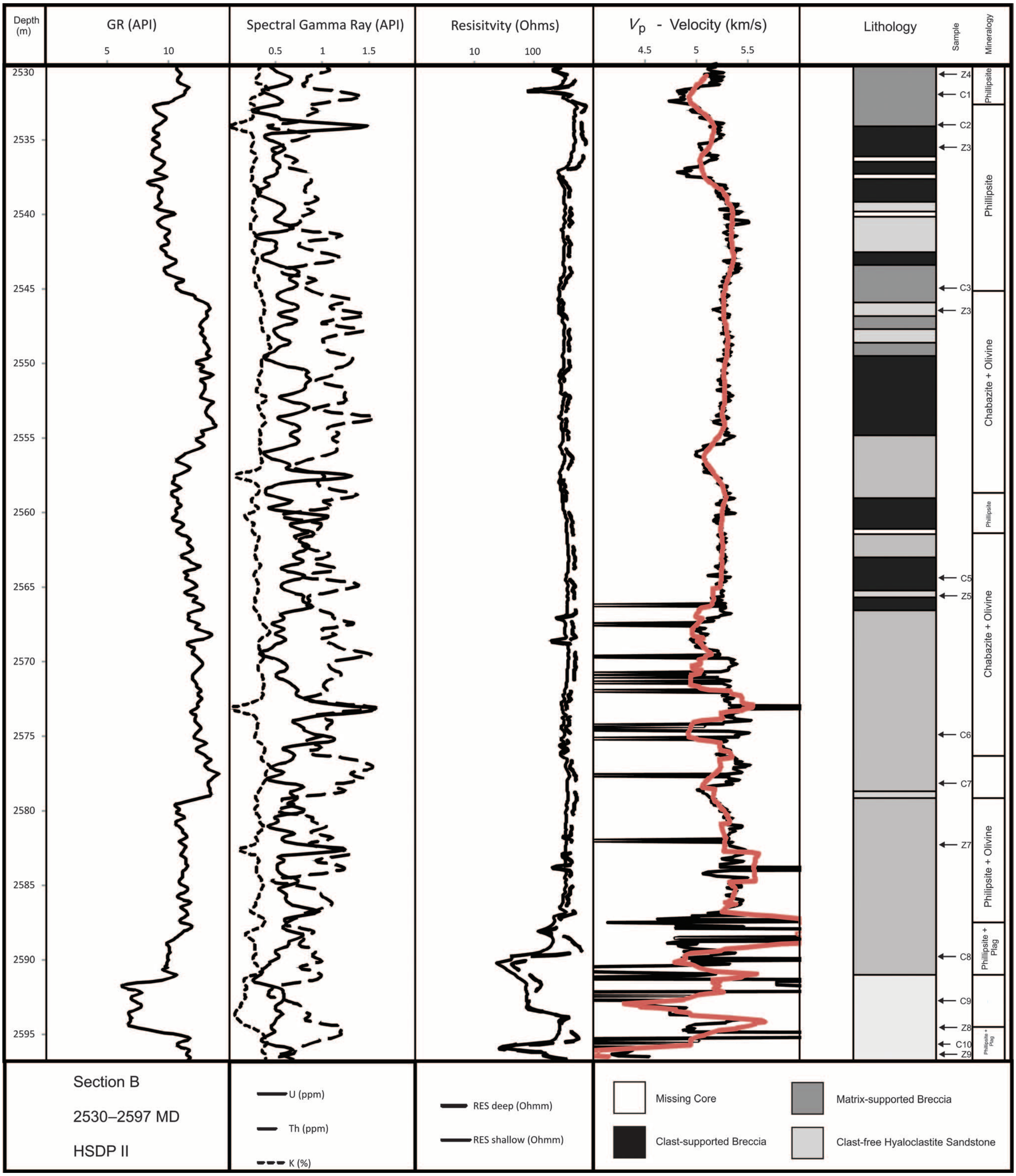

Figure 9. Composite log, sample intervals, and mineralogical observations from core section B. A density log was not recorded for the Hawaiian Scientific Drilling Project phase II borehole.

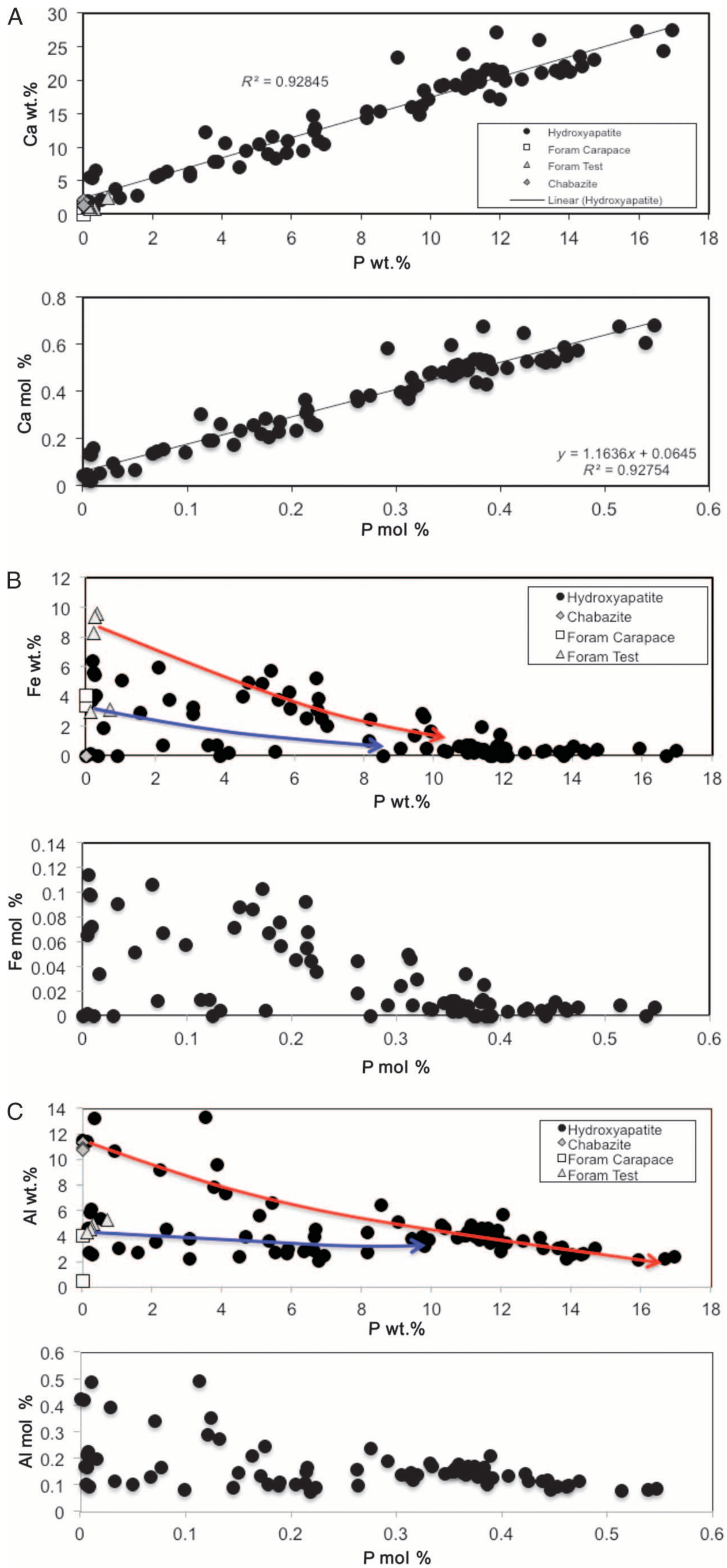

Figure 10. (A) Calcium weight and mole percentage for suspected hydroxyapatite EDX sample points. A good linear trend is observed in both cases, which indicates that the formation of calcium and phosphorus are mutually beneficial and the gradient of the line suggesting hy. (B) Iron weight and mole percentage versus phosphorus weight and mole percentage for suspected hydroxyapatite samples. Two trends are observed: one from high iron values reflecting chabazite replacement and one from low iron values reflecting bioclast replacement. (C) Aluminum weight and mole percentage versus phosphorus weight and mole percentage for suspected hydroxyapatite samples. A good linear trend is observed in both cases. Two trends are seen: one from chabazite samples losing aluminum and one constant value from bioclasts that already had low aluminum.

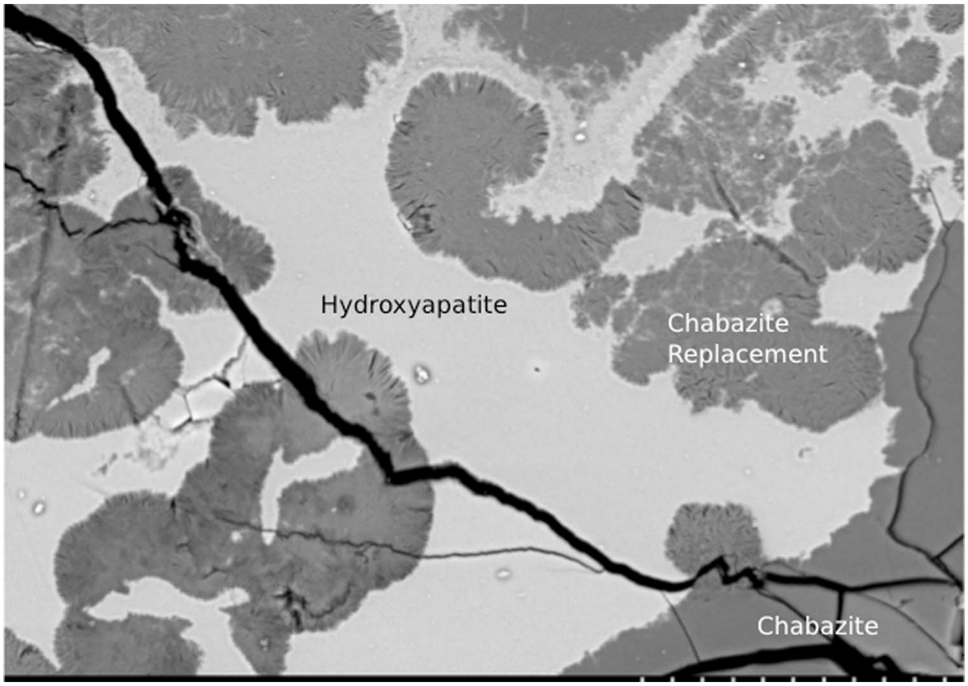

Figure 11. C7 site 5a 800× magnification image width 200 μm. YAGBSE (yttrium aluminum garnet back scattered electron) image showing a highly magnified image of phosphorus-rich hydroxyapatite intergrowths (white). Residual chabazite enclosed as darker blobs.

APPENDIX 2: IDENTIFICATION OF HYDROXYAPATITE

Recognition of Hydroxyapatite in Hawaiian Scientific Drilling Project II

Spot energy-dispersive x-ray weight and mole percentage values can be plotted for common elements in phosphate-enriched suspected hydroxyapatite zones (Figure 10A–C). A linear increase exists in both the mole and weight percentage of Ca/P for all suspected hydroxyapatite samples. Hydroxyapatite can form via bioclast replacement (Baker et al., 1998). In the HSDP II, logged sections (A and B) foraminifera are found within the fine-grained hyaloclastite horizons associated with hydroxyapatite growth. Foraminifera test and carapace values for Ca and P are low; however, P is still present, suggesting it has been leached after bioclast replacement has occurred (Figure 10A). In Figure 7, the highest concentration of P occurs at the rim, with the alteration front pervasive through the sample gradually replacing the chabazite structure. Therefore, the gradient of the mole concentration linear trend characterizes the alteration from chabazite to hydroxyapatite. Therefore, at a set P value, for example, 0.2 Ca values equal 0.3. Then the calculated gradient of approximately 0.6 suggests that for every 10 Ca molecules, 6 P molecules are present, so given the common hydroxyapatite structure $[C_{10}(PO_4)_6(OH)_2]$, this suggests that the phosphorus-enriched zone is in fact hydroxyapatite.

Other P relationships are not as clear. Both Fe and Al are reduced with increases in P that suggest a replacement process. Two trends exist in each of the data sets: for Fe, there is a low weight percentage trend from foraminifera carapaces and a high weight percentage trend from foraminifera tests (Figure 10B). This may suggest differential rates of replacement to P-rich hydroxyapatite depending on the type of bioclast undergoing replacement. The Al trend reflects either a replacement in the original foraminifer bioclast or subsequent alteration of the chabazite structure (removing Al). This gives rise to two trends: an abrupt decrease in Al, which is removed from the chabazite structure; and a constant low Al value, which is already low in the foraminifer test. Both of these trends are also reflected in the mole percentage of each sample (Figure 10C).

Replacement

Replacement of zeolite for P-rich hydroxyapatite occurs in proximity to foraminifera tests. At 800× magnification, it is possible to resolve the textures between apatite (lightest color) and chabazite (darkest color) (Figure 11). Figure 7 showed a gradual increase in P away from the margin, if a void. At this resolution, dendritic fingers of hydroxyapatite spread into the sample and then join. This produces small transitional (shared EDX characteristics of chabazite and hydroxyapatite) blobs with irregular margins, which form the Al and Fe trends in Figure 10B and C. The alteration front in all samples does not follow a fracture plane in the chabazite structure. Titanium oxides were not observed in this study, although they are a common accessory mineral that occurs with zeolites (Walton and Schiffman, 2003).